

Comparison of filters for detecting gravitational wave bursts in interferometric detectors

Nicolas Arnaud, Matteo Barsuglia, Marie-Anne Bizouard, Violette Brisson, Fabien Cavalier, Michel Davier, Patrice Hello,*
Stephane Kreckelbergh, Edward K. Porter, and Thierry Pradier

Laboratoire de l'Accélérateur Linéaire, Boîte Postale 34, Bâtiment 200, Campus d'Orsay, 91898 Orsay Cedex, France

(Received 30 October 2002; published 28 March 2003)

Filters developed in order to detect short bursts of gravitational waves in interferometric detector outputs are compared according to three main points. Conventional receiver operating characteristics (ROC) are first built for all the considered filters and for three typical burst signals. Optimized ROC are shown for a simple pulse signal in order to estimate the best detection efficiency of the filters in the ideal case, while realistic ones obtained with filters working with several “templates” show how detection efficiencies can be degraded in a practical implementation. Second, estimations of biases and statistical errors on the reconstruction of the time of arrival of pulse-like signals are then given for each filter. Such results are crucial for future coincidence studies between gravitational wave detectors but also with neutrino or optical detectors. As most of the filters require a pre-whitening of the detector noise, the sensitivity to a nonperfect noise whitening procedure is finally analyzed. For this purpose lines of various frequencies and amplitudes are added to a Gaussian white noise and the outputs of the filters are studied in order to monitor the excess of false alarms induced by the lines. The comparison of the performances of the different filters finally show that they are complementary rather than competitive.

DOI: 10.1103/PhysRevD.67.062004

PACS number(s): 04.80.Nn, 07.05.Kf

I. INTRODUCTION

Long baseline interferometric detectors of gravitational waves (GW) [1–4] are currently taking their first data. The preparation for data analysis of compact binary inspiral signals, the most promising source of GW to date, with these new instruments has been in progress for a long time, as well as for periodic sources (see, e.g. [5] for a review). The effort concerning the search for burst sources is more recent. The expected GW burst sources are primarily massive star collapse either with neutron star (NS) [6–12] or black hole (BH) formation [13]. The duration of such events is at most a few milliseconds and the simulated amplitudes do not exceed a few 10^{-23} (NS formation) or 10^{-22} (BH formation) for sources located at about 10 Mpc. With these typical amplitudes, interferometric detectors of the first generation have no hope of “seeing” such events if they occur beyond the Galaxy [12,14]. Other sources of GW bursts are NS binary [15–20] or BH binary mergers [21–25], for which a large amount of effort is currently underway in order to predict plausible waveforms. More exotic, but detectable by first generation interferometers, are possible GW bursts emitted by cosmic strings [26].

All the predicted sources of GW bursts are in fact characterized by a very rough knowledge of the emitted waveforms. Unless simulations of core collapse or binary mergers can provide accurate waveforms (which seems currently doubtful), the use of matched filtering, which would be the optimal method in case of perfect knowledge of the waveforms, is not possible. Suboptimal filtering methods are then required for detecting GW bursts. Such methods have been developed in different groups in the last few years. The excess power monitoring has been built upon in successive

versions [27–30]. Time frequency methods are also planned for burst signal or noise non-stationarity detection [31–34]. In our group, we have developed filtering methods with the idea of being as robust as possible with respect to the possible signal waveforms [14,35–37]. We have also introduced a benchmark test in order to compare different filters [14] in a given situation. This benchmark is, however, incomplete if we want to fully understand the different methods. The goal of this paper is then to compare the different proposed filters. A filter based on the moving average [38] is added to the bank of previously published filters. The definitions of the filtering methods are first recalled. We intentionally discard some of them, such as bin counting [14] or the norm of the autocorrelation [39], which are clearly not competitive compared to the others. The efficiency curves (detection probability vs false alarm rate) of the different filters for generic burst signals with various signal-to-noise ratios (SNR) are then computed. We first use optimal versions of the filter (in the sense that the filter parameters are matched to the signal) and secondly realistic implementations for each filter, with different “templates” working in parallel. In the following part, the timing properties of the filters (bias and statistical timing accuracies) are studied with respect to both signal SNR and signal width. The sensitivity of the filters to the noise whitening quality is finally discussed.

II. FILTERS FOR DETECTING GW BURSTS

In this section we firstly describe the noise model we will use in all the following sections and then we enumerate and briefly describe the filtering methods.

A. The noise model

Throughout the paper we assume that the noise is Gaussian and white with zero mean. The standard deviation of the noise is then

*Email address: hello@lal.in2p3.fr

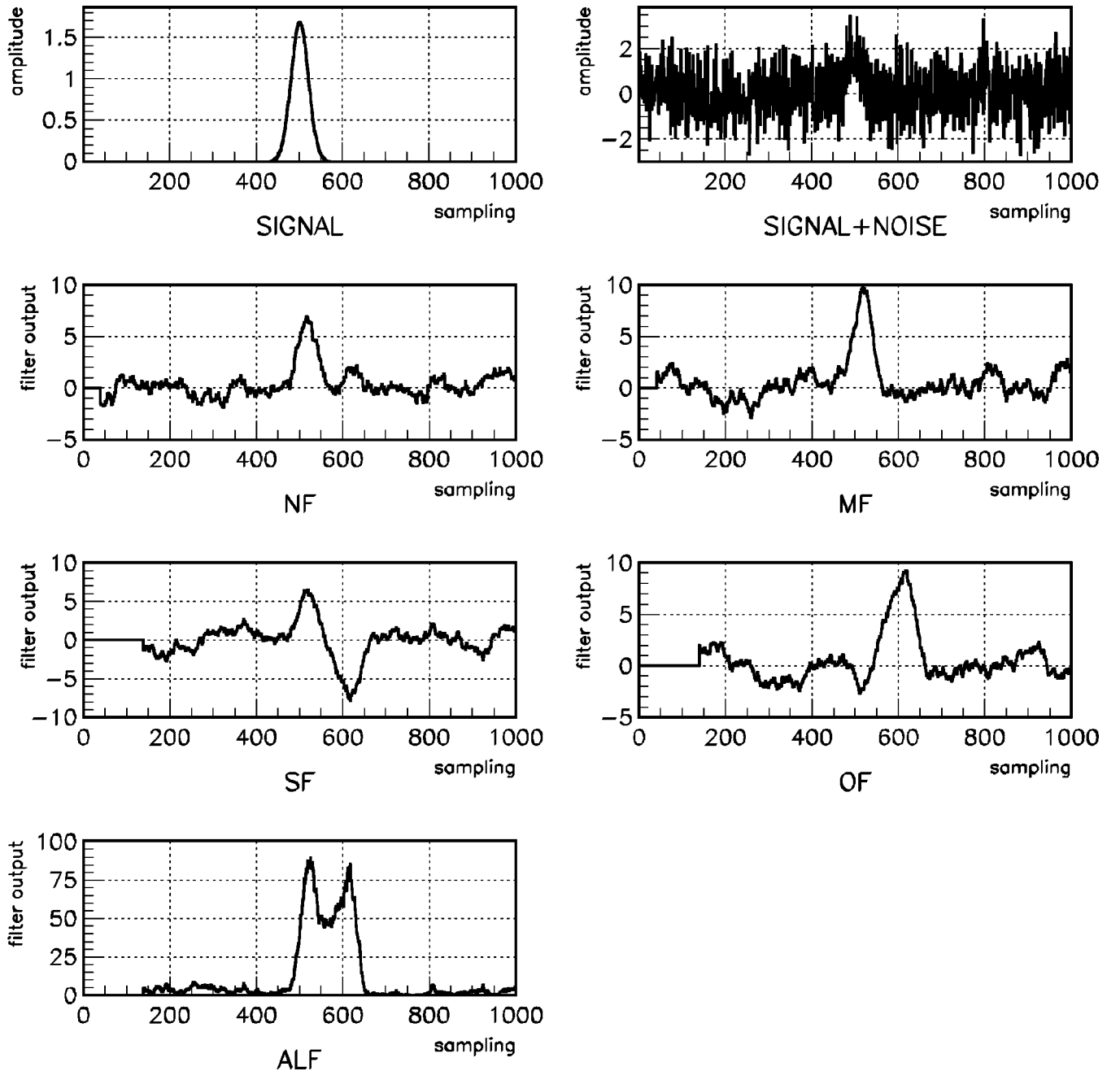


FIG. 1. Responses of the filters to a Gaussian burst signal of half-width 1 ms (upper left panel) embedded in noise (upper right panel) which is assumed to be white Gaussian with zero mean and unity standard deviation. The five following plots show the responses of the norm filter (NF), the mean filter (MF), the slope filter (SF), the offset filter (OF) and the ALF. For each filter the moving window size is chosen to be optimal: $N=40$ (corresponding to the signal width $N/f_0 \approx 2$ ms) for the NF and the MF and $N=140$ for the ALF and related filters. In this example, the optimal SNR is 10; the maximal NF SNR is about 6.9, the maximal MF SNR is about 9.7, the maximal SF SNR is about 7.8 and the maximal OF SNR is about 9.3. The maximal ALF (quadratic) SNR is here about 40. We note in each case the obvious time delay between the signal peak and the output maximum. This will cause a trivial bias when we study the filters' time resolution (see Sec. IV).

$$\sigma = \sqrt{\frac{S_h f_0}{2}}, \quad (2.1)$$

where f_0 is the sampling frequency and S_h is the one-sided spectral density of the noise. For numerical examples, we take $f_0=20$ kHz (Virgo sampling rate) and $\sqrt{S_h} \approx 4 \times 10^{-23}/\sqrt{\text{Hz}}$, which is about the minimum value of the

foreseen noise spectral density of the Virgo interferometer [40]; this choice is correct since the minimum is located in the frequency range for the expected burst sources of GW. The fact that we choose Gaussian noise is not essential, but simply convenient for the design of the filters. Deviation from Gaussianity will produce, for example, an excess in the rate of false alarms and it will then be possible, for example,

TABLE I. Distances of detection and performances of the different filters in detecting a sample of supernovae signals. NF=norm filter, MF=mean filter, SF=slope filter, OF=offset filter. The results are extracted from Ref. [37], except for the new MF results, indicated by bold print.

Filter	Optimal	NF	SF	OF	ALF	MF
Average distance (kpc)	27.4	11.5	11.3	15.2	22.5	20.0
Performance	1	0.46	0.49	0.59	0.81	0.78

to retune the algorithms thresholds according to the real noise statistics. In the frequency range of interest, above a few 100 Hz, the Virgo noise sensitivity curve is rather flat, although not exactly white. Most of the filtering methods presented here and in [14] require a whitening of the noise [41,42], which is foreseen for the Virgo data processing output. In the following, we normalize the noise level by its standard deviation, so that we are dealing with a Gaussian noise with zero mean and unit standard deviation. We also denote the data x_i at sample times i/f_0 . Let us recall also that we conventionally define a signal to noise ratio (SNR) after filtering as (filter output m_o) / σ_o , where m_o and σ_o are the mean and standard deviation of the filter output in the absence of a signal. Of course a SNR can have different dimensionality depending on whether the filter is linear or quadratic, for instance. This shows at least that the SNR is an ambiguous criterion when we are interested in comparing different filters, linear or not.

B. The norm filter

The norm filter [14] is a simple version of the excess power statistics [27]. It is based upon a monitoring of the local signal energy in a moving window

$$y_k = \sum_{i=k}^{k+N-1} x_i^2. \quad (2.2)$$

Under this form, the filter appears to be nonlinear with a single parameter, the moving window size N . In the presence of noise only, y_k is distributed as a χ^2 variable with N degrees of freedom (mean N and standard deviation $\sqrt{2N}$). The variable

$$y_k^{NF} = \sqrt{2y_k} - \sqrt{2N-1} = \sqrt{2 \times \sum_{i=k+1}^{k+N} x_i^2} - \sqrt{2N-1} \quad (2.3)$$

can be very well approximated by a standard normal variable, if $N \geq 30$ [43]. This is the definition of the norm filter (NF). We note of course that y_k^{NF} is normalized so that it is well a SNR. The response of the NF to a test signal is displayed in Fig. 1. The NF is able to recover about 70% of the optimal SNR in this example.

C. The slope filters and the ALF

A family of filters based upon fitting a straight line to the data has been proposed [37]. The two (nonindependent) results of the fit, namely the line slope a and the offset value b

$$a = \frac{\langle tx \rangle - \langle t \rangle \langle x \rangle}{\langle t^2 \rangle - \langle t \rangle^2}, \quad (2.4)$$

$$b = \langle x \rangle - a \langle t \rangle = \langle x \rangle - \frac{\langle tx \rangle - \langle t \rangle \langle x \rangle}{\langle t^2 \rangle - \langle t \rangle^2} \langle t \rangle \quad (2.5)$$

where $\langle x \rangle = (1/N) \sum_{i=1}^N x_i$ and $t_i = i/f_0$, can be used as linear filters with variances

$$\sigma_a^2 = \frac{12f_0^2}{N(N^2-1)}, \quad (2.6)$$

$$\sigma_b^2 = \frac{4N+2}{N(N-1)}. \quad (2.7)$$

The normalized slope filter (SF) and offset filter (OF), namely $y_k^{SF} = a/\sigma_a$ and $y_k^{OF} = b/\sigma_b$, can be uncorrelated by diagonalization of the covariance matrix, yielding

$$y_k^\pm = \frac{y_k^{SF} \pm y_k^{OF}}{\sqrt{2(1 \pm \alpha)}}, \quad (2.8)$$

with correlation coefficient

$$\alpha = -\sqrt{\frac{3}{2} \left(\frac{N+1}{2N+1} \right)}. \quad (2.9)$$

The two uncorrelated filters can finally be combined and the ALF (nonlinear) filter is obtained:

$$y_k^{ALF} = (y_k^+)^2 + (y_k^-)^2 = \frac{(y_k^{SF})^2 + (y_k^{OF})^2 - 2\alpha y_k^{SF} y_k^{OF}}{1 - \alpha^2}. \quad (2.10)$$

In the presence of noise only, the ALF is well approximated with a χ^2 distributed random variable with 2 degrees of freedom, hence a mean and a standard deviation both equal to 2. The only parameter is N in all cases. Again, simple recurrence relations can be used in the successive calculations of the SF and OF (and so for the ALF) outputs. The responses of the SF, OF and ALF to a test signal are shown on Fig. 1. The moving window size for each filter is optimally chosen to be $N=140$, which is about 7 times the signal half-width as stated in [37]. We see that the OF performs better in detecting the signal than the SF in this example. As already noticed, the ALF (quadratic filter) and the other (linear) filters do not have the same ‘‘dimension,’’ since the ALF outputs are proportional to the energy of the signal and not to the amplitude, hence the much larger SNR for the ALF.

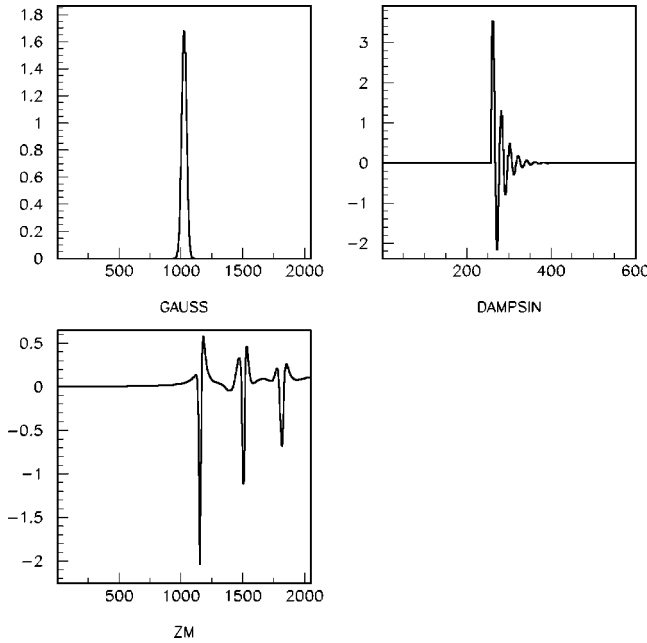


FIG. 2. The signals used for the ROC. Upper left: Gaussian pulse with half-width 1 ms. Upper right: damped sine with frequency 1 kHz and damping time 1 ms. Lower: signal emitted by core collapse as simulated by Zwerger and Müller. In the plots, each signal would have an optimal SNR $\rho_0 = 10$ if added to a white noise with unity rms.

D. The mean filter

We now introduce the mean filter (MF), which is nothing but the filtering by moving the average or the boxcar average [38]. The mean filter computes the mean of the data in a moving window

$$y_k^{MF} = \frac{1}{N} \sum_{i=k}^{k+N-1} x_i. \tag{2.11}$$

It is a linear filter with a single parameter, the window size N . In the presence of noise only, y_k^{MF} is distributed as a Gaussian random variable with zero mean and standard deviation $1/\sqrt{N}$. The computation of the filter outputs is very fast, as trivial recursive relations between y_k^{MF} and y_{k+1}^{MF} can be used. So the moving window can be allowed to move bin by bin, without concern for CPU time. The response of the MF to a test signal is displayed in Fig. 1. We see that the MF is able to recover almost all of the optimal SNR in this example.

A first means of comparing the filters is to benchmark them within common conditions, i.e. subjecting them to the same GW signals for identical noise conditions. We first used a benchmark based on a catalogue of 78 supernovae signals, simulated by Zwerger and Müller (ZM) [8,44] in the axisymmetric case (see [14] and [37] for details).

The results of this first benchmark for the different filters are collected in Table I. We recall those already shown in Ref. [37] and add the new one for the mean filter. We note that the MF has a performance similar to the ALF's.

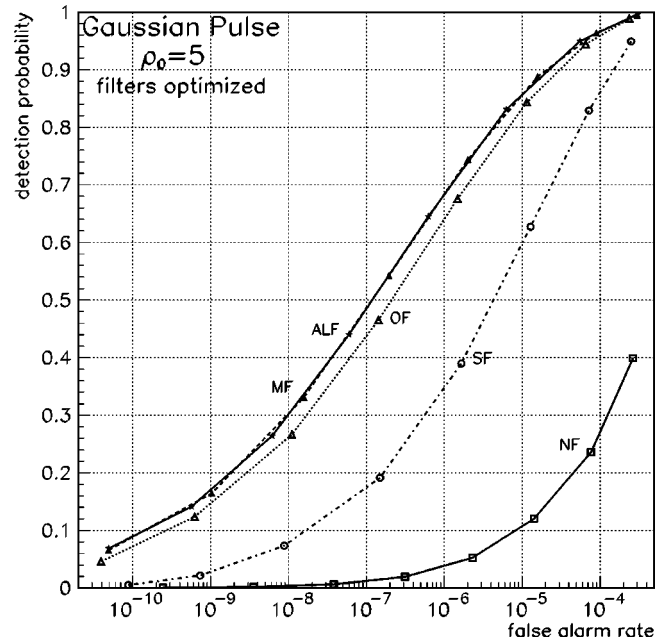


FIG. 3. ROC for optimized filters. The signal is a Gaussian pulse of half-width 1 ms with optimal SNR $\rho_0 = 5$. Black star (\star): the ALF; white triangle (\triangle): the OF; white circle (\circ): the SF; black triangle (\blacktriangle): the MF; and white square (\square): the NF. The false alarm rate is a false alarm probability *per bin*, as in all other ROC.

III. EFFICIENCY OF THE FILTERS

Unfortunately the previous benchmark gives only a partial view of filters performances, as it is computed for a specified false alarm rate. Of course one would wish to extend the comparison of filters to other false alarm rates, especially for

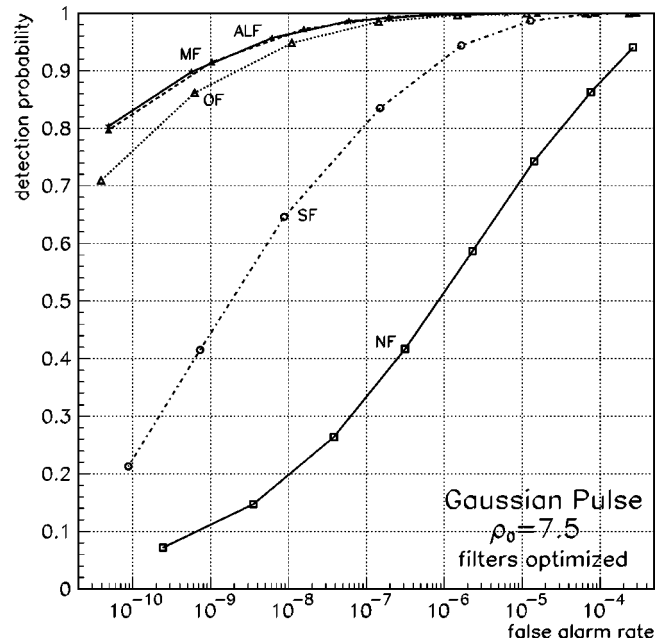


FIG. 4. ROC for optimized filters. The signal is a Gaussian pulse of half-width 1 ms with optimal SNR $\rho_0 = 7.5$. The symbols are \star (ALF), \triangle (OF), \circ (SF), \blacktriangle (MF) and \square (NF).

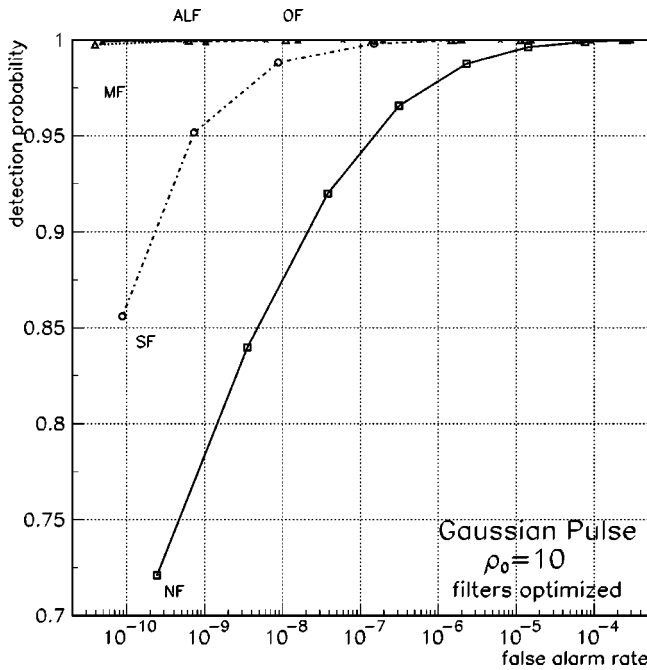


FIG. 5. ROC for optimized filters. The signal is a Gaussian pulse of half-width 1 ms with optimal SNR $\rho_0=10$. The symbols are \star (ALF), \triangle (OF), \circ (SF), \blacktriangle (MF) and \square (NF). For such a signal amplitude, the ALF, the OF and the NF have efficiencies very close to 1, even for very small false alarm rates.

those lying in the likely range allowed during science runs of interferometers. Such a tool is standard in signal processing, the so-called receiver operating characteristics (ROC), which displays the curves detection efficiency vs the false alarm rate. In the next section we will compute the ROC for typical (albeit of course arbitrary) burst signals. This will complete our understanding of the detection power of the filters.

A. Methodology

For each filter we compute the ROC for three distinct typical burst-like signals. The first is a Gaussian pulse of half-width $w=1$ ms of the form

$$s(t) = A \exp\left(-\frac{(t-t_0)^2}{2w^2}\right). \quad (3.1)$$

The second is a damped sinusoid of frequency $f=1$ kHz and damping time $\tau=1$ ms of the form

$$s(t) = AH(t-t_0) \exp[-(t-t_0)/\tau] \sin[2\pi f(t-t_0)], \quad (3.2)$$

where $H(x)$ is the Heaviside step function [$H(x)=0$ if $x < 0$ and $H(x)=1$ if $x > 0$].

The last waveform is a supernova signal from the ZM catalogue (number 6 in order of decreasing simulated signal energy) [8]. The three signals are displayed in Fig. 2. The amplitude A of each of these three signals is calibrated according to the corresponding optimal SNR ρ_0 (if one of the signals were detected by optimal filtering with the same noise conditions then the mean optimal SNR would be ρ_0).

TABLE II. Choice of the 10 window sizes to be implemented in parallel for the MF and the NF, and for the SF, the OF and the ALF. The corresponding typical signal widths are also given.

Signal size (ms)	0.5	0.75	1	1.25	1.5	2	2.5	3.5	7.5	10
MF, NF	10	15	20	25	30	40	50	70	150	200
SF, OF and ALF	35	50	75	90	105	140	175	250	500	750

We have used for the Monte Carlo simulations a data window of size 2048. For each simulated data window, we first pass the filters with noise only. If one of the filters is triggered then we increment its false alarm counter, or we add one of the signals to the noise and look if the filter detects the signal, in which case its detection counter is incremented. The efficiency of a filter in detecting one of the signals is then the ratio of the number of detections by the number of noise realizations without false alarm. Meanwhile, the false alarm rate is the ratio of noise realizations with a false alarm to the total number of noise realizations and then divided by the data window size, resulting in a false alarm rate per bin. The data window size (2048 bins) has in fact been chosen large enough to contain the signals but not too large in order to have a very low probability of having more than one false alarm in a single window. This obviously may occur only for very high false alarm rates (not reached in practice). We first study the case of optimized filters (only one “template” matched to the signal we consider) in order to have information about the maximal efficiencies the filters can reach. We then study the case of realistic implementations, with several “templates” working in parallel. It is worth noting that the

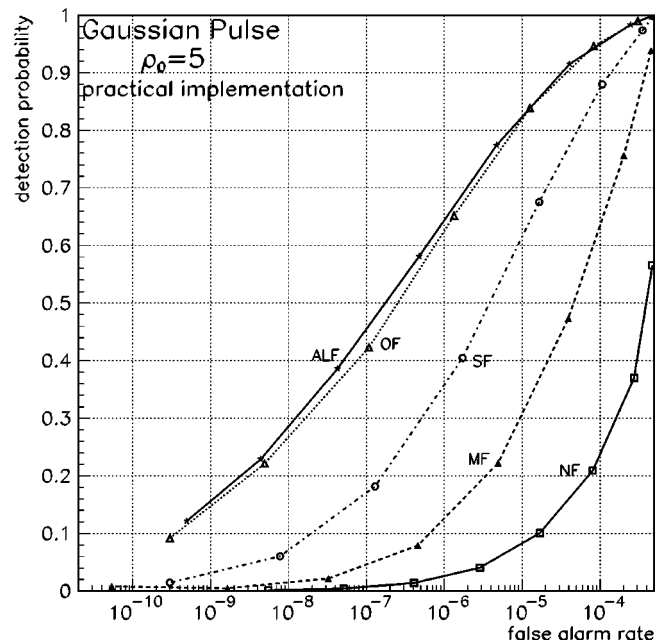


FIG. 6. ROC for filters in a realistic implementation. The signal is a Gaussian pulse of half-width 1 ms with optimal SNR $\rho_0=5$. The symbols are \star (ALF), \triangle (OF), \circ (SF), \blacktriangle (MF) and \square (NF).

TABLE III. False alarm rates κ_{50} for which a filter efficiency reaches about 50% for a Gaussian pulse of half-width 1 ms and optimal SNR $\rho_0=5$. The figures are extracted from Figs. 3 (optimized filters) and 6 (realistic filters).

Filter	ALF	OF	SF	MF	NF
Optimized filters	10^{-7}	2×10^{-7}	2×10^{-6}	10^{-7}	$> 2 \times 10^{-4}$
Realistic filters	2×10^{-7}	3×10^{-7}	4×10^{-6}	4×10^{-5}	4×10^{-4}

“event” notion introduced in [37] is here automatically taken into account, as the detection algorithm stops (and the detection counter is incremented) as soon as the filter output is above threshold. The method is thus independent of the real number of bins above threshold and of the details of event clustering, as defined in [37].

B. ROC for optimized filters

We first consider optimized filters, in the sense that their parameters (essentially the moving window size N) are optimally matched to the signal. We consider for this purpose the Gaussian pulse signal [Eq. (3.1)]. With $w=1$ ms, the filters are matched with window sizes $N=40$ (MF and NF) or $N=140$ (SF, OF and ALF). The ROC for various optimal SNRs are shown in Figs. 3, 4 and 5 ($\rho_0=5, 7.5$ and 10 , respectively). For each SNR value, the MF and the ALF show very close efficiencies. While much simpler, the MF is able to compete with the ALF for detecting pulse-like signals. However, this is the ideal situation, all filters being optimally implemented with respect to the signal. We will see how this is modified with realistic implementations in the next section. Concerning the ALF, it is again clear that we gain in combining the OF and the SF (in the ALF), as the OF

and the SF are always less efficient ALF whatever the false alarm rate or the signal strength. Between the OF and the SF, the OF is always significantly more efficient than the SF. Finally the NF appears as noncompetitive for detecting short pulses even in its optimized version. In particular, in the case of low SNR ($\rho_0=5$) the NF efficiency is close to zero for practical false alarm rates in the interferometers (say $< 10^{-6}$). For higher SNR ($\rho_0=10$), the NF cannot reach 50% efficiency in the false alarm rate range we study. On the contrary for such a SNR, the MF and the ALF have efficiencies near 100% over all the range of false alarm rates.

C. ROC for practical implementations of the filters

In the preceding section the filters were matched for a single pulse width. In the real world, however, the signal (if any) width will not be known in advance. Moreover, the signal itself will surely not be a perfect Gaussian pulse. That is why the filters must be implemented with different “templates” in order to conveniently cover the signal parameter space. For all the filters here, the only parameter is the moving window size. Thus in practice the filters will be implemented (for instance, in the online trigger system) with different moving windows in parallel. Such an implementation is shown in Table II, where the typical burst width ranges

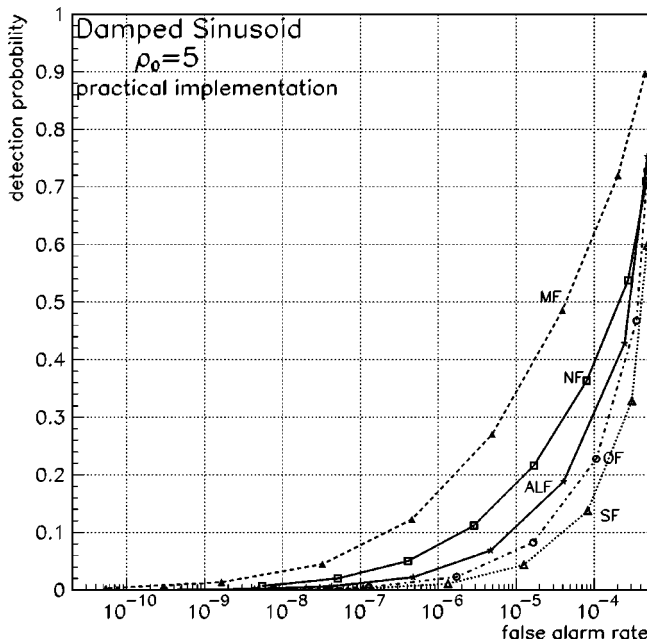


FIG. 7. ROC for filters in a realistic implementation. The signal is a damped sine of frequency 1 kHz and damping time 1 ms with optimal SNR $\rho_0=5$. The symbols are \star (ALF), Δ (OF), \circ (SF), \blacktriangle (MF) and \square (NF).

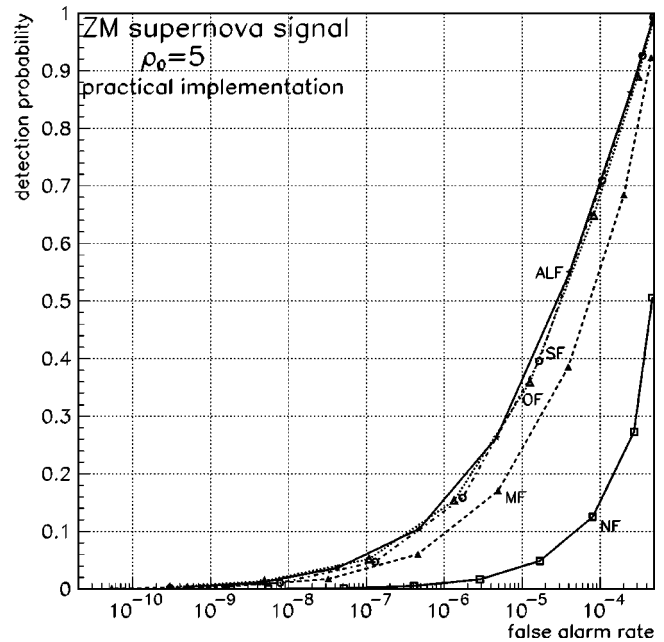


FIG. 8. ROC for filters in a realistic implementation. The signal is a supernova simulated signal with optimal SNR $\rho_0=5$. The symbols are \star (ALF), Δ (OF), \circ (SF), \blacktriangle (MF) and \square (NF).

TABLE IV. False alarm rates κ_{50} for which the filter efficiency reaches about 50% for the 3 signals with optimal SNR $\rho_0=5$. For each signal the best κ_{50} value is marked (\star). The results for the OF and the SF are not reported in the table since their detection efficiencies are always less than the ALF ones (by construction).

	ALF	MF	NF
Gauss (ideal)	10^{-7} (\star)	10^{-7} (\star)	$>2 \times 10^{-4}$
Gauss (realistic)	2×10^{-7} (\star)	4×10^{-5}	4×10^{-4}
Damped sine (realistic)	3×10^{-4}	4×10^{-5} (\star)	2×10^{-4}
ZM (realistic)	3×10^{-5} (\star)	7×10^{-5}	5×10^{-4}

from 0.5 ms to 10 ms. For the NF and the MF the window sizes correspond to the signal widths Δt ($N = \Delta t \times f_0$), while for the ALF, the SF and the OF they correspond to about 3.5 times the signal widths [37].

The ROC for the Gaussian pulse of half-width 1 ms are shown in Fig. 6. The optimal SNR is 5 (the most interesting to exhibit filters differences with the false alarm rates considered). Note that the signal width corresponds exactly to one of the window sizes of the implementation ($N=40$ for the NF and the MF and $N=140$ for the slope filters family). When compared to Fig. 3, the realistic situation differs from the ideal one in particular for the MF. The ALF is the most efficient, followed by the OF and the SF, while the NF is always the worst. The case of the MF is interesting: its efficiency is excellent if matched to the pulse width but it dramatically decreases if implemented with several “templates.” The matched template ($N=40$ here) is always as efficient in detecting the pulse but the other templates contribute to increase the number of false alarms. For the other filters the increase of false alarms due to the mismatched templates is much less. This can be also exhibited by comparing the false alarm rates κ_{50} for which the filter efficiency reaches 50%. Note that κ_{50} can be also a good quality criterion for comparing the different filters. The results are shown in Table III.

The sensitivity of the overall false alarm rate to the number of templates is then a problem for the MF while the other filters seem much more robust with respect to this aspect. Indeed their efficiency curves shift only slightly to the right if we compare Figs. 6 and 3, or their κ_{50} changes by only a factor roughly about 2. For MF the shift is again very large and its κ_{50} changes by a factor of about 400.

The next ROC for the damped sine signal are plotted on Fig. 7. The situation is completely different than before. If compared to Fig. 6, the MF has about the same efficiency, while the NF is significantly better. But for this signal, the ALF and parent filters are the worst. The 50% efficiencies are obtained for false alarm rates $\kappa_{50} \approx 4 \times 10^{-5}$ for the NF (about the same as for the Gaussian signal), $\kappa_{50} \approx 2 \times 10^{-4}$ for NF (twice as good) and about $\kappa_{50} \approx 3 \times 10^{-4}$ for the ALF, that is 10^3 worse than for the Gaussian signal. In this configuration the ALF is not competitive while the MF is the best filter in the list.

Finally the ROC for the supernova signal are shown on Fig. 8. We find roughly the hierarchy first obtained with the Gaussian pulse. The ALF and related filters are the most efficient, the MF arrives next and the least efficient is the NF. The 50% efficiencies are here obtained for false alarm rates

about $\kappa_{50} \approx 3 \times 10^{-5}$ for the ALF, the OF and the SF, $\kappa_{50} \approx 7 \times 10^{-5}$ for the MF and $\kappa_{50} \approx 5 \times 10^{-4}$ for the NF.

D. Discussion

The first point to mention is that the relative efficiencies of the different filters depend strongly on the type of waveform. For instance, the ALF is not suited to the detection of the damped sine signal above. The MF and the NF have very roughly the same detection efficiencies whatever the signal, so in this sense these filters are robust. However, the ALF can be much more efficient than the MF and the NF. In all cases we find that the ALF is always more efficient than the SF and the OF. We effectively gain a lot in combining the SF and the OF in the ALF. In its optimized version (N matched to the signal size), the MF can be as efficient as the ALF (see Fig. 3), but the efficiency falls dramatically with a practical implementation. The MF is, however, the most efficient for the damped sine signal. The NF is never the most efficient for any signal but it appears more efficient than the ALF in

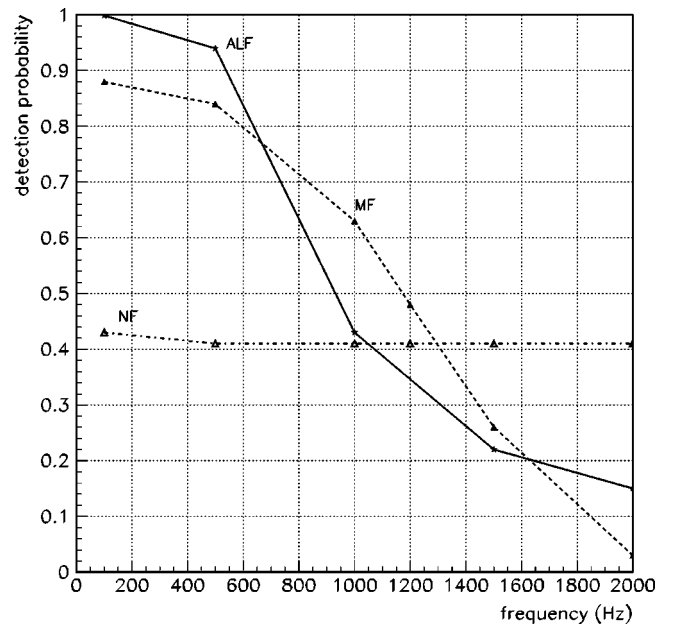


FIG. 9. Detection efficiency of the MF, the NF and the ALF in their practical implementation for a damped sine signal of damping time $\tau = 100$ ms and varying frequency. The signals optimal SNR is $\rho_0 = 5$ and the filter thresholds used here correspond to a common false alarm rate of about 5×10^{-4} . We note the robustness of the NF while the ALF and the NF efficiencies decrease with increasing frequency.

detecting the damped sine signal. All these results are summarized in Table IV where the false alarm rates for 50% detection efficiency for all the signals are given.

It may appear surprising that the MF performs better than the NF or the ALF in detecting the damped sinusoidal waveform, as the mean of a sinusoid is 0. In fact, the MF is efficient because one of its “templates” width is well adapted to detect one of the signal peaks. In fact, a cutoff frequency may be associated with each of the templates of length N through $f_c = f_0/N$, where f_0 is again the sampling frequency. For the implementation shown in Table II, the largest cutoff frequency (associated with the lowest value of N) is $f_c^{MAX} \approx 1$ kHz. Below this frequency, there will be always at least one template short enough to pick out only one signal peak. On the contrary, above f_c^{MAX} , all the templates average the signal cycles and the MF output dramatically decreases. A similar behavior is found for the ALF, due to the fact that the mean slope of a sinusoid with many cycles is zero. This can be seen in Fig. 9, where the detection efficiencies of the MF, the NF and the ALF for the same false alarm rate are shown as a function of the frequency of a damped sine signal of damping time $\tau = 100$ ms (long enough to have many cycles when the frequency is high enough). We see clearly that the ALF and the MF are very efficient at low frequency, while they dramatically lose efficiency as the signal frequency increases. On the contrary the NF efficiency is almost constant, whatever the signal frequency. This shows some robustness for the NF. We note also that for the signal frequency $f = 1$ kHz, the MF is again more efficient than the NF and the ALF, as in Fig. 7, while its efficiency tends towards 0 as the signal frequency becomes larger and larger.

IV. TIMING ISSUES

A. Methodology

The filter timing properties are very important since timing accuracy is necessary (1) for validating coincidences between GW detectors, and (2) for reconstructing the signal. For instance, the signal time delay between VIRGO and LIGO-Hanford is up to 27 ms. Thus, the estimation accuracy of the time of arrival of a signal obtained with a given filter must be much less than this delay. This timing accuracy is also crucial in the case of coincidences with neutrino detectors. In the latter case, GW timing accuracy needs to be below 1 ms in order to not limit the measurement of neutrino masses [45].

The definition of a time-of-arrival estimator can be in general nontrivial since it depends both on the filter and on the signal waveform. That is why we will use in fact a simple waveform in order to evaluate the optimal performance of a filter to measure a signal time of arrival, keeping in mind that for a real signal the timing accuracy should be degraded.

In order to evaluate the timing accuracy of the filters we proceed as follows. We consider as a burst signal a Gaussian pulse [Eq. (3.1)] with a variable amplitude A (always calibrated according to the optimal SNR ρ_0) and a time width w . The signal is buried in white Gaussian noise and the filters try to detect it. We define the expected time of arrival as the maximum of the pulse, that occurs at t_0 for the signal of Eq.

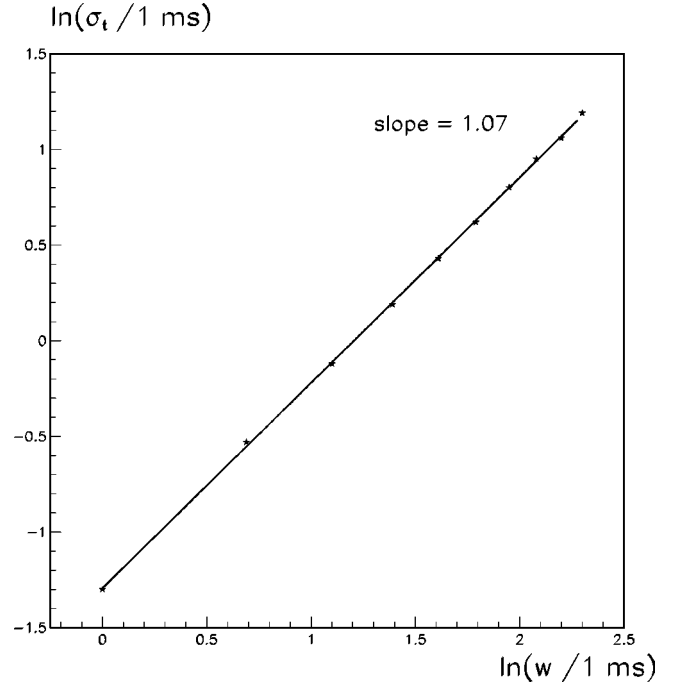


FIG. 10. The NF statistical error for time of arrival reconstruction as a function of the signal duration in log-log scales. The slope is about 1.08, larger than for the optimal filter as well as for all the other filters.

(3.1). The first arrival time estimator considered for the filters is given by the SNR maximum. A different estimator will be in fact used for ALF. After many noise realizations we can thus estimate the systematic bias Δt (mean of the distribution of measured times of arrival) if any and the statistical error σ_t (rms of the distribution) on t_0 for a given set of parameters (w and ρ_0).

In the case of optimal filtering (here correlation of the noisy Gaussian pulse with an identical Gaussian pulse template that is nothing but the peak correlator [14] with a single template) no systematic bias is found and the statistical error is [46]

$$\sigma_t \approx 0.145 \text{ ms} \left(\frac{w}{1 \text{ ms}} \right) \left(\frac{\rho_0}{10} \right)^{-1}. \quad (4.1)$$

We note that the statistical error is linear with respect to both w and $1/\rho_0$. This timing accuracy is, in fact, the best that can be achieved (optimal filtering). We see that for the canonical example, $w = 1$ ms and $\rho_0 = 10$, $\sigma_t \approx 0.15$ ms, well below the time delay between interferometers or the required accuracy for coincidences with neutrinos. The question is then to investigate if the studied suboptimal filters retain acceptable timing accuracies. The bias and statistical errors on the measure of t_0 *a priori* depend on the amplitude ρ_0 and on the width w of the pulse signal. For every filter, we will then study both Δt and σ_t as functions of ρ_0 and w . We will use the matched versions of the filters (window size N matched to the signal width w) so the numbers given are to be considered as upper limits, which are best achieved, in principle, with the filters.

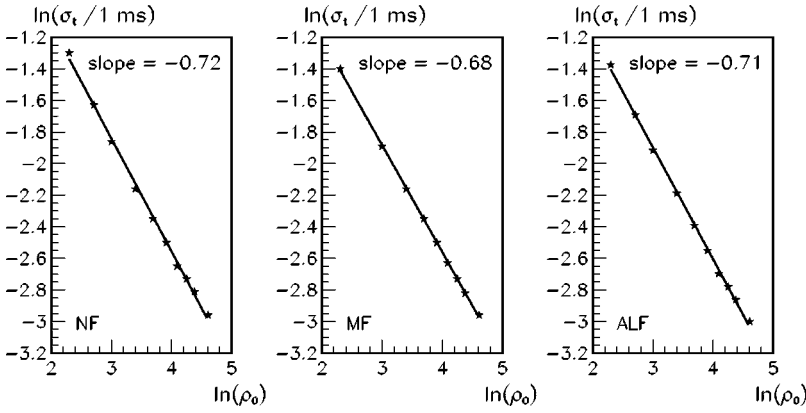


FIG. 11. The statistical errors for time of arrival reconstruction as a function of the signal amplitude ρ_0 in log-log scales for the NF, the MF and the ALF. In the case of the NF, the slope is about -0.72 , worse than for the optimal filter, while it is about -0.68 for the MF (a little worse than the NF) and about -0.71 for the ALF (similar to the NF).

B. Norm filter

For the norm filter, we first find a systematic bias $\Delta t = (N/2) \times$ sampling time. This shift is simply related to the window size N and can be easily corrected for. The correction can itself be incorporated in the filter definition so it plays no role. The statistical error has less trivial relations with the signal parameters. Figures 10 and 11 (left panel) show the behavior of σ_t as a function of ρ_0 and w , respectively. The statistical error does not behave linearly either with $1/\rho_0$ or with w , contrarily to the optimal filter. In log-log scales, however, the curves are linear and the slopes can be obtained from a least squares fit. They differ substantially from unity and are, of course, larger than the (plus or minus unity) slopes found in the case of optimal filter. The results can be combined into a single expression for the statistical error

$$\sigma_t \approx 0.273 \text{ ms} \left(\frac{w}{1 \text{ ms}} \right)^{1.07} \left(\frac{\rho_0}{10} \right)^{-0.72}. \quad (4.2)$$

C. Mean filter

For the mean filter, we find exactly the same systematic effect as for the NF, $\Delta t = (N/2) \times$ sampling time. Again this bias can be corrected for and is unimportant. The statistical error σ_t is first found to behave linearly with respect to the signal width w (better than the NF). But, as for the NF, σ_t is not linear with respect to $1/\rho_0$, as shown in Fig. 11 (middle panel). The slope of the curve σ_t vs ρ_0 in log-log scales is about -0.68 , well above -1 as for the optimal filter, but a little worse than the NF. We can combine the results into a single expression:

$$\sigma_t \approx 0.246 \text{ ms} \left(\frac{w}{1 \text{ ms}} \right) \left(\frac{\rho_0}{10} \right)^{-0.68}. \quad (4.3)$$

TABLE V. Statistical errors for the time of arrival estimation for a Gaussian pulse with width $w = 1$ ms and amplitude normalized to $\rho_0 = 10$.

Filter	Optimal	ALF	OF	SF	MF	NF
σ_t (ms)	0.15	0.25	0.31	0.24	0.25	0.27

We note that for the canonical values $\rho_0 = 10$ and $w = 1$ ms, we obtain $\sigma_t \approx 0.25$ ms, about the same as for the NF (about 0.27 ms), which is, of course, larger than the optimal filter statistical error, but not much larger.

D. The ALF and related filters

For the SF and the ALF, the response to a pulse signal shows two peaks as seen in Fig. 1. The peak maxima are in principle symmetric relatively to t_0 . We consequently define the time of arrival new estimator as $\tilde{t}_0 = (t_1 + t_2)/2$ where t_1 and t_2 are the time locations of the two peaks. For the OF the situation is “normal” (a single maximum) as for the NF and the MF and the time of arrival estimator is not modified. For the three filters SF, OF and ALF we find again the usual systematic $\Delta t = (N/2) \times$ sampling time, which we can correct for. Then the behavior of the statistical error σ_t is found to be linear with respect to the signal size w , even for the nonlinear filter ALF. Finally, as for NF and MF, the three filters do not have a linear behavior with respect to $1/\rho_0$. Figure 11 (right panel) shows the curves σ_t vs ρ_0 for the ALF (results for the SF and the OF are not displayed). In each case the slope in log-log scales is well below -1 and similar to what has been found for the NF and the MF, which is around -0.7 . The results are combined into the following formulas:

$$\sigma_t^{SF} \approx 0.244 \text{ ms} \left(\frac{w}{1 \text{ ms}} \right) \left(\frac{\rho_0}{10} \right)^{-0.69}, \quad (4.4)$$

$$\sigma_t^{OF} \approx 0.311 \text{ ms} \left(\frac{w}{1 \text{ ms}} \right) \left(\frac{\rho_0}{10} \right)^{-0.68}, \quad (4.5)$$

$$\sigma_t^{ALF} \approx 0.253 \text{ ms} \left(\frac{w}{1 \text{ ms}} \right) \left(\frac{\rho_0}{10} \right)^{-0.71}. \quad (4.6)$$

E. Discussion

The first and important point is that all the suboptimal filters studied in this paper have good timing accuracies. The systematic bias for the time of arrival is trivial and can be easily corrected for. The statistical errors are, of course, larger than in the case of optimal filtering but are still acceptable. For the canonical example, $w = 1$ ms and $\rho_0 = 10$ (see

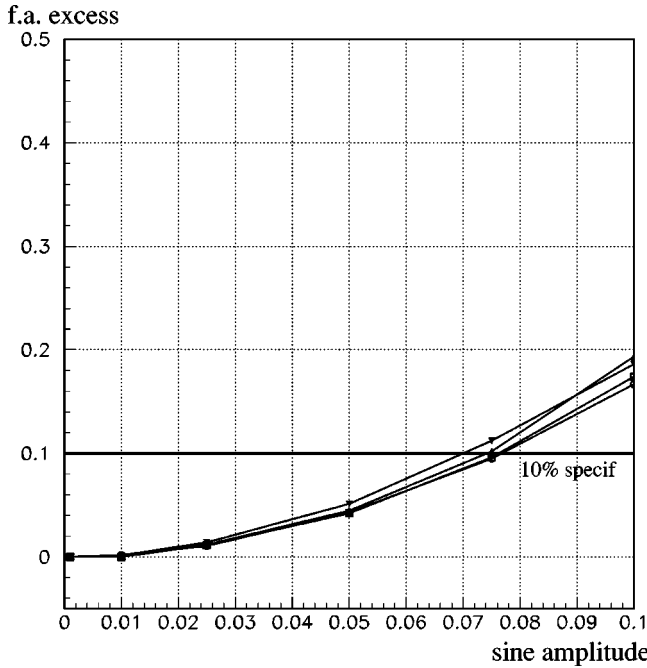


FIG. 12. The relative false alarm excess for the norm filter (implemented with $N=50$) for lines of different frequencies as a function of the line amplitude measured in σ units (the Gaussian white noise rms). The different frequencies are 0.6 Hz (\blacktriangle), 100 Hz (\blacktriangledown), 200 Hz (\circ) and 400 Hz (\square). We note that the false alarm excess is grossly independent of the line frequency.

Table V), the statistical error is about 0.15 ms for optimal filtering, about the same for the ALF, the SF, the MF and the NF (around 0.25 ms) and the worst is obtained for the OF, about 0.3 ms, which is twice the optimal value. In any case, in this example, the timing accuracy is well below 1 ms for all the filters.

We then note that all linear filters behave linearly with respect to the signal width. For the nonlinear filters, the ALF also displays such a behavior (as a descendant of two linear filters) while the NF does not. All the suboptimal filters have a nonlinear behavior with respect to $1/\rho_0$, the best one here being the NF (slope closest to -1), but the difference between the filters is not really significant as the slopes range from -0.68 for the MF and the OF to -0.71 for the ALF and -0.72 for the NF.

Finally, balancing all the aspects, the best filter concerning timing accuracy seems to be the ALF, the NF being penalized by its nonlinearity with respect to the signal width. This conclusion was not *a priori* obvious, considering the definition and the broad response of the ALF filter (see Fig. 1). However, this optimistic conclusion should be moderated. Indeed, this result has been obtained with a simple waveform, a single peak. With a more structured signal (a supernova signal), the situation is in fact less favorable. The first problem is to properly define a time of arrival estimator. Different estimators have been tested in a Monte Carlo simulation for determining the time of arrival of ZM signals with the ALF [39]: time of maximum SNR, time of first bin above threshold, average time between two SNR peaks etc. All of

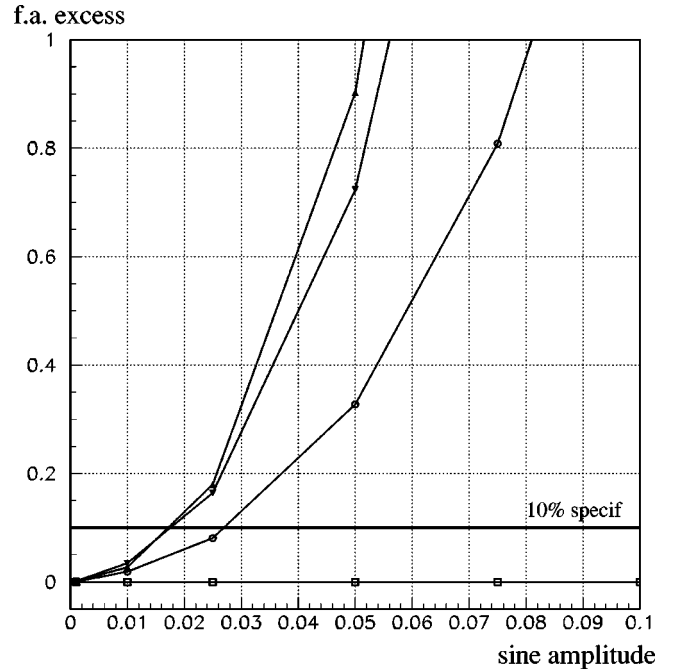


FIG. 13. The relative false alarm excess for the mean filter (implemented with $N=50$) for lines of different frequencies as a function of the line amplitude measured in σ units (the Gaussian white noise rms). The different frequencies are 0.6 Hz (\blacktriangle), 100 Hz (\blacktriangledown), 200 Hz (\circ) and 400 Hz (\square). We note that the false alarms excess decreases with increasing frequencies, until it completely vanishes for frequencies above the cutoff frequency corresponding to the window size N . Here $N=50$ corresponds to a time size of 2.5 ms and to a cutoff frequency of 400 Hz.

them have been found to be biased. Moreover, the bias may strongly depend on the waveform type (types I, II or III as classified by Zwerger and Müller [8]). The smallest bias, averaged over all the waveforms of the ZM catalogue, is about 0.5 ms for signal SNR of 5. Type III signals have the largest contribution to this bias (with biases around 1.6 ms in average). This shows that the ALF timing accuracy (bias + statistic error) can be in some cases significantly larger than 1 ms. This can have serious consequences, for example, in the case of coincidences with neutrino detectors. Indeed, if the GW timing accuracy is worse than about 1 ms, the determination of neutrino masses is degraded [45].

V. EFFECT OF LINES ON THE FILTER FALSE-ALARM RATES

The suboptimal filters studied in this paper require a pre-whitening of the noise. In reality, noise whitening is never perfect and we need to quantify the filters sensitivity to imperfect whitening. This has been already done for the ALF [37] but needs to be extended to the other filters. For this purpose, about 100 h of *Gaussian* white noise data are simulated and a single frequency component of the form $A \sin(2\pi ft)$ (that can mimic a large line residual) is added. We then filter the data (Gaussian white noise+line) with the different algorithms (including the ALF in order to be able to compare the filters in exactly the same situations) using slic-

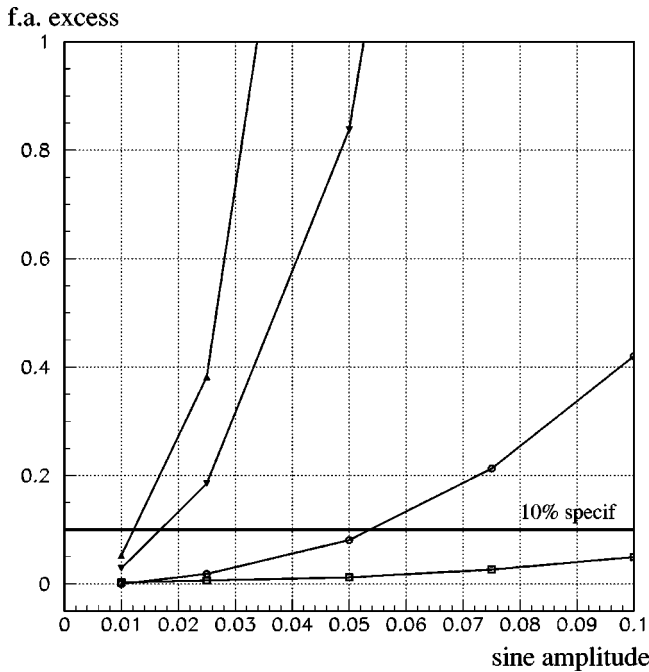


FIG. 14. The relative false alarm excess for the ALF (implemented with $N=170$ that is matched to 2.5 ms signals as for the MF and the NF) for lines of different frequencies as a function of the line amplitude measured in σ units (the Gaussian white noise rms). The different frequencies are 0.6 Hz (\blacktriangle), 100 Hz (\blacktriangledown), 200 Hz (\circ) and 400 Hz (\square). We note that the false alarms excess decreases with increasing frequencies.

ing windows and we record the effective number of false alarms for each one as functions of A and f . In the following, a nominal false alarm rate of 10^{-6} is chosen. So for 100 h of data sampled at 20 kHz about 7200 ± 85 false alarms are expected (the standard deviation of about 85 is estimated from a binomial law). For instance, we find $n_0 = 7138$ false alarms with the MF for the 100 h of only Gaussian white noise. For each filter, we then increase the sine amplitude A , measure the new number of false alarms n each time and compute the relative excess of false alarms with respect to the ideal situation ($A=0$), i.e. the quantity $(n - n_0)/n_0$. The results for the NF, the MF and the ALF are given in Figs. 12, 13 and 14, respectively. We investigate as examples four different frequencies: 0.6 Hz, corresponding to the natural pendulum mode frequency of the suspended mirrors in VIRGO, and 100 Hz, 200 Hz and 400 Hz, corresponding to power line harmonics or wire resonances. The filters window sizes have been chosen to be $N=50$ for both the NF and the MF and $N=170$ for the ALF, so that all window sizes correspond to the same matched signal size (about 2.5 ms). The results for the three filters are quite different. For the NF the curves for the false alarms excess vs A are about the same whatever the line frequency. In contrast, for the MF and the ALF, the false alarm excess strongly depends on the line frequency, from very large excess at low frequency to lower or even vanishing at higher frequencies. For the MF we find again the effect of the cutoff frequency associated with the window size N , $f_c = f_0/N$. Above this cutoff frequency, the line does not increase anymore the number of false alarms

and has simply no effect on the MF performance, since, by construction, the MF averages the fast oscillations in the window and the net effect is zero. The same phenomenon appears also, but to a lesser extent, for the ALF. We can now set a specification for the whitening procedure, such as the excess in the false alarm rate does not exceed the nominal value more than 10%. For the NF this implies that the whitened line amplitudes must be lower than 7–8% of the ideal Gaussian white noise rms σ for all frequencies. For the MF and the ALF, the effect depends on the frequency. For example, for the important 0.6 Hz frequency in VIRGO, the specification is that the line amplitude should be less than about 2% of the noise rms for the MF and about 1% for the ALF. For increasing frequencies the specifications become less and less stringent until they can be totally relaxed above the cutoff frequency. Such specifications (from 1% to 10% of ideal noise rms for line amplitudes) seem quite severe. Let us define the noise flatness [41]

$$\xi = \frac{\exp\left(\frac{2}{f_0} \int_0^{f_0/2} \ln S_h(f) df\right)}{\frac{2}{f_0} \int_0^{f_0/2} S_h(f) df}, \quad (5.1)$$

where $S_h(f)$ is the noise one-sided power spectral density (PSD). The flatness is such that $\xi \in [0; 1]$, the extremal values being reached for a very peaky PSD ($\xi \approx 0$) and for a white PSD ($\xi \approx 1$). The most stringent requirement (for the 0.6 Hz pendulum mode) corresponds to a maximal line amplitude at about 1% of the background Gaussian and white noise. If we convert this in terms of noise flatness we obtain a specification [39] that reads $\xi \geq 0.97$. This may seem very demanding at first sight, but it is within the reach of existing whitening algorithms that can already achieve a level of $\xi > 0.98$ [41].

Asking for no more than 10% extra false alarms due to imperfect noise whitening is in fact not very demanding as far as detection probability is concerned. Indeed, we can correct for the false alarm excess of 10% (in order to recover the desired false alarm rate) by fine tuning of the detection thresholds. But relaxing the requirements to 20% or 50% does not really change the situation at least for the low frequency lines. For the MF and the ALF the specifications on low frequency line amplitudes will always be a few % of the background noise rms since the increase of false alarms is a very sharp function of the line amplitude.

Of course the number of false alarms considered so far is the raw number, i.e. the number of outputs above threshold. However, as the consecutive outputs of filters are not independent and once a filter is triggered by noise alone, we find in practice not only a single but a number of consecutive outputs above threshold that correspond to the same false alarm event. We can thus redefine an *event* as proposed in [37]. A false alarm event is then no longer a simple filter output above threshold but a cluster of successive outputs above threshold, at most separated by the correlation length of the filter. For example, for the simulated 100 h of data, without lines added, we find for the ALF (with threshold

= 27.85) 7208 raw false alarms that are resolved in 1170 false alarm events, so a reduction factor about 6. When lines are added it has been checked that one order of magnitude on the false alarm rate is gained if we take the new definition of a false alarm event. This can then relax somewhat the constraints on the line amplitudes. As an example, for the 0.6 Hz line with amplitude $A = 7.5 \times 10^{-2} \times \sigma$, we find more than 63,000 false alarms in the 100 h of noisy data, giving only 6361 false alarm events, still below the nominal false alarms number (7208) for the 100 h of data free of lines.

To be complete let us finally mention that the shapes of the curves *relative false alarm event excess vs the line amplitude* are in fact very close to the previous curves (with the brut false alarm excess). That means that, if we first have set the desired absolute false alarm rate to some value and if we set the specifications on the whitening quality in asking again no more than 10% false alarms in excess, we will find about the same specifications for remaining line amplitudes, whatever the false alarm definition.

VI. CONCLUSIONS

In this paper the principles of GW burst detection algorithms previously studied in our group have been recalled. The mean filter, based on moving average, has been introduced. Their performances for detecting a set of simulated supernova signals have been completed and summarized. This was until now the only way to compare the different filters. We have then considered three other tools or criteria in order to fully understand and compare the filters. Firstly we have systematically made use of the conventional ROC in detecting typical burst signals. Secondly, the timing properties (systematic biases and statistical errors in timing reconstruction) have been evaluated. Finally we have studied the effect of a nonperfect whitening (remaining spectral lines) on the effective false alarm rate of the filters.

Concerning the old benchmark, the ALF and the mean

filter show the best performance in detecting the supernova signals of the Zwerger and Müller catalogue. When looking at the ROC, the ALF and the mean filter are still ahead provided they can be optimized, meaning that the signal length is known in advance. In practical situations, where banks of filters are used in order to cover the signal sizes space, the situation is not as clear. In particular, for short damped sine signals, the ALF is much less efficient than the mean filter and even the norm filter. A characteristic feature of the mean filter as well as the norm filter is their relative robustness: their efficiency curves are very similar from one signal to another. The ALF is much less robust; it is in general (much) better but in some cases it is the worst performing. Concerning the timing issues, all the filters have similar timing accuracies, worse (but no more than a factor 2) than the optimal filter timing accuracy. The main concern is maybe about the whitening quality which is required by most of the algorithms. Indeed the remaining line amplitudes are required to stay below a fraction of the ideal background Gaussian white rms. Fortunately the redefinition of a false alarm event allows one to gain almost one order of magnitude on the effective resulting false alarm rate. Finally, taking everything into account, it is difficult to state that one filter is better than the others. Rather than establishing some hierarchy, as done, for example with our previous benchmark, the important conclusion of this paper is that the different filters are in fact complementary. This is indeed manifest when we again look at the different ROC: a single filter cannot be the most efficient for all burst signals. Then rather than using a single “preferred” filter, it is advisable to operate a battery of different filters having their own qualities and defects. The next step is then to develop a strategy to find the best use of all the filters in the battery.

As we have presented in this paper an unbiased way to estimate the performance of filters, we would like to suggest its application in the context of the development of GW burst detection methods. This could be very valuable in order to directly compare the performances of different filters and their complementarity or redundancy.

-
- [1] A. Abramovici, W.E. Althouse, R.W.P. Drever, Y. Gürsel, S. Kawamura, F.J. Raab, D. Shoemaker, L. Sievers, R.E. Spero, K.S. Thorne, R.E. Vogt, R. Weiss, S.E. Whitcomb, and M.E. Zucker, *Science* **256**, 325 (1992).
 - [2] B. Caron *et al.*, *Nucl. Phys. B (Proc. Suppl.)* **54B**, 167 (1997).
 - [3] K. Danzmann *et al.*, in *Gravitational Wave Experiments*, edited by E. Coccia, G. Pizzella, and F. Ronga (World Scientific, Singapore, 1995).
 - [4] Masaki Ando *et al.*, *Phys. Rev. Lett.* **86**, 3950 (2001).
 - [5] B.F. Schutz, in *The Detection of Gravitational Waves*, edited by D.G. Blair (Cambridge University Press, Cambridge, England, 1991).
 - [6] R. Mönchmeyer, G. Schäfer, E. Müller, and R.E. Kates, *Astron. Astrophys.* **246**, 417 (1991).
 - [7] S. Bonazzola and J.-A. Marck, *Astron. Astrophys.* **267**, 623 (1993).
 - [8] T. Zwerger and E. Müller, *Astron. Astrophys.* **320**, 209 (1997).
 - [9] M. Rampp, E. Müller, and M. Ruffert, *Astron. Astrophys.* **332**, 969 (1998).
 - [10] H. Dimmelmeier, J.A. Font, and E. Müller, *Astrophys. J. Lett.* **560**, L163 (2001).
 - [11] H. Dimmelmeier, J. A. Font, and E. Müller, *Class. Quantum Grav.* **19**, 1291 (2002).
 - [12] H. Dimmelmeier, J.A. Font, and E. Müller, *Astron. Astrophys.* **393**, 523 (2002).
 - [13] R.F. Stark and T. Piran, *Phys. Rev. Lett.* **55**, 891 (1985).
 - [14] N. Arnaud, F. Cavalier, M. Davier, and P. Hello, *Phys. Rev. D* **59**, 082002 (1999).
 - [15] K. Oohara and T. Nakamura, in *Relativistic Gravitation and Gravitational Waves*, edited by J.-A. Marck and J.-P. Lasota (Cambridge University Press, Cambridge, England, 1997).
 - [16] F.A. Rasio and S.L. Shapiro, *Class. Quantum Grav.* **16**, R1 (1999).
 - [17] M. Ruffert and H.-Th. Janka, *Astron. Astrophys.* **338**, 535 (1998).

- [18] H.-T. Janka, T. Eberl, M. Ruffert, and C.L. Fryer, *Astrophys. J. Lett.* **527**, L39 (1999).
- [19] H.-T. Janka and M. Ruffert, in the Proceedings of the Conference on Stellar Collisions, Mergers and their Consequences, ASP Conference series, edited by M. Shara.
- [20] M. Ruffert and H.-Th. Janka, *Astron. Astrophys.* **380**, 544 (2001).
- [21] M. Alcubierre, W. Bengert, B. Bruegmann, G. Lanfermann, L. Nergler, E. Seidel, and R. Takahashi, *Phys. Rev. Lett.* **87**, 271103 (2001).
- [22] M. Shibata and K. Uryu, *Prog. Theor. Phys.* **107**, 265 (2002).
- [23] J. Baker, M. Campanelli, and C. Lousto, *Phys. Rev. D* **65**, 044001 (2002).
- [24] J. Baker, M. Campanelli, C. Lousto, and R. Takahashi, *Phys. Rev. D* **65**, 124012 (2002).
- [25] S. Husa, Y. Zlochower, R. Gomez, and J. Winicour, *Phys. Rev. D* **65**, 084034 (2002).
- [26] T. Damour and A. Vilenkin, *Phys. Rev. D* **64**, 064008 (2001).
- [27] E.E. Flanagan and S.A. Hughes, *Phys. Rev. D* **57**, 4535 (1998).
- [28] W.G. Anderson, P.R. Brady, J.D.E. Creighton, and E.E. Flanagan, *Int. J. Mod. Phys. D* **9**, 303 (2000).
- [29] W.G. Anderson, P.R. Brady, J.D.E. Creighton, and E.E. Flanagan, *Phys. Rev. D* **63**, 042003 (2001).
- [30] A. Viceré, *Phys. Rev. D* **66**, 062002 (2002).
- [31] W.G. Anderson and R. Balasubramanian, *Phys. Rev. D* **60**, 102001 (1999).
- [32] S.D. Mohanty, *Phys. Rev. D* **61**, 122002 (2000).
- [33] L. Fabbroni and M. Vannucci, "Wavelet tests for the detection of transients," VIRGO note VIR-NOT-FIR 1390 151, 2000.
- [34] J. Sylvestre, *Phys. Rev. D* **66**, 102004 (2002).
- [35] N. Arnaud, F. Cavalier, M. Davier, P. Hello, and T. Pradier, to appear in the Proceedings of the XXXIVth Rencontres de Moriond on "Gravitational Waves and Experimental Gravity," Les Arcs, 1999, gr-qc/9903035.
- [36] T. Pradier, N. Arnaud, M.-A. Bizouard, F. Cavalier, M. Davier, and P. Hello, *Int. J. Mod. Phys. D* **9**, 309 (2000).
- [37] T. Pradier, N. Arnaud, M.-A. Bizouard, F. Cavalier, M. Davier, and P. Hello, *Phys. Rev. D* **63**, 042002 (2001).
- [38] A. Papoulis, *Signal Analysis* (McGraw-Hill, New York, 1977), p. 343.
- [39] T. Pradier, Ph.D. thesis, LAL 01-15, Université de Paris-Sud, Orsay, 2001.
- [40] <http://www.virgo.infn.it/senscurve/>
- [41] E. Cuoco, G. Calamai, L. Fabbroni, G. Losurdo, M. Mazzoni, R. Stanga, and F. Vetrano, *Class. Quantum Grav.* **18**, 1727 (2001).
- [42] E. Cuoco, G. Losurdo, G. Calamai, L. Fabbroni, M. Mazzoni, R. Stanga, G. Guidi, and F. Vetrano, *Phys. Rev. D* **64**, 122002 (2001).
- [43] M.R. Spiegel, *Probabilités et Statistiques* (McGraw-Hill, Paris, 1981).
- [44] <http://www.mpa-garching.mpg.de/~ewald/GRAV/grav.html>
- [45] N. Arnaud, M. Barsuglia, M.-A. Bizouard, F. Cavalier, M. Davier, P. Hello, and T. Pradier, *Phys. Rev. D* **65**, 033010 (2002).
- [46] N. Arnaud, M. Barsuglia, M.-A. Bizouard, P. Canitrot, F. Cavalier, M. Davier, P. Hello, and T. Pradier, *Phys. Rev. D* **65**, 042004 (2002).